JAMES | Journal of Advances in Modeling Earth Systems

RESEARCH ARTICLE
10.1029/2023MS003616

Alleviated WRF Summer Wet Bias Over the Tibetan Plateau Using a New Cloud Macrophysics Scheme

Dingchi Zhao[1], Yanluan Lin[1], Wenhao Dong[2], Yi Qin[3,4], Wenchao Chu[1], Kun Yang[1], Husi Letu[5], and Lei Huang[1]

[1]Ministry of Education Key Laboratory for Earth System Modeling, Department of Earth System Science, Tsinghua University, Beijing, China, [2]NOAA/Geophysical Fluid Dynamics Laboratory, Princeton, NJ, USA, [3]Lawrence Livermore National Laboratory, Livermore, CA, USA, [4]Pacific Northwest National Laboratory, Richland, WA, USA, [5]State Key Laboratory of Remote Sensing Science, The Aerospace Information Research Institute, Chinese Academy of Sciences (CAS), Beijing, China

Abstract Reliable precipitation simulation over the Tibetan Plateau (TP) remains a challenge, manifested by a prominent systematic wet bias in the warm season. Previous studies have generally neglected the potential linkage between surface radiation energy budget and precipitation bias. Prevalent scattered cumulus and thunderstorms over the TP in summer strongly influence surface radiation. A cloud fraction scheme considering subgrid temperature and humidity fluctuations is implemented in the WRF model and tested for a month-long simulation. It is found that the scheme better reproduces the surface solar radiation compared to a default cloud fraction scheme in the WRF model. Using abundant surface observations, we find that overestimation of the downward surface shortwave radiation (DSSR) would lead to wet bias. DSSR overestimation contributes to higher surface temperature and larger evaporation and enhanced atmospheric instability, which favor more simulated convective precipitation. The study suggests that a better simulation of clouds and surface radiation would benefit precipitation simulation over the plateau.

Plain Language Summary Summer precipitation over the Tibetan Plateau (TP) is generally overestimated in general circulation models as well as regional weather forecasts and climate models. The prevailing "popcorn-like" clouds over the TP in summer would strongly impact surface radiation. Considering the potential linkage between surface radiation energy budget and precipitation bias, a statistical cloud fraction and subgrid condensation scheme (GS-PDF scheme) is implemented in the WRF model and tested for a month-long simulation. The GS-PDF scheme better captures clouds over the TP with more mid-low cloud water (ice) than the default Xu-Randall scheme. Increased mid-low cloud water in the GS-PDF scheme reduced simulated downward surface shortwave radiation, reduced simulated surface temperatures, atmospheric instabilities and convective precipitation, leading to alleviated wet bias over the TP. This study suggests that better simulations of cloud and surface radiation would be beneficial for simulations of hydrological cycles over the TP.

Key Points:

- A new cloud macrophysics scheme considering subgrid temperature and humidity fluctuations is implemented in the WRF model
- The new macrophysics scheme reduced simulated downward surface shortwave radiation, surface temperatures and atmospheric instabilities
- A better simulation of clouds and surface radiation would benefit precipitation simulation over the Tibetan Plateau

Supporting Information:

Supporting Information may be found in the online version of this article.

Correspondence to:

Y. Lin,
yanluan@tsinghua.edu.cn

Citation:

Zhao, D., Lin, Y., Dong, W., Qin, Y., Chu, W., Yang, K., et al. (2023). Alleviated WRF summer wet bias over the Tibetan Plateau using a new cloud macrophysics scheme. *Journal of Advances in Modeling Earth Systems*, *15*, e2023MS003616. https://doi.org/10.1029/2023MS003616

Received 4 FEB 2023
Accepted 25 AUG 2023

1. Introduction

Located in the eastern part of the subtropical Afro-Eurasian continent, the Tibetan Plateau (TP), regarded as "the Roof of the World," is the highest plateau in the world with an area of about 3.1×10^6 km^2 and an average elevation over 4,000 m above sea level. Its dynamic and thermodynamic effects have great impacts on the downstream and global climate (Fu et al., 2020; Liu et al., 2020; Wu et al., 2020; Zhao et al., 2019). The TP also has the most massive glacier and ice outside the polar regions, and plays a critical role in the hydrological cycle and the water supplies in Asia (Qiu, 2008; Xu et al., 2008, 2019). It is the headstream of more than 10 of Asia's major rivers, which provide critical freshwater for nearly 40% of the world's population for domestic, agricultural, and industrial use (L. Wang et al., 2021; Yao et al., 2019). Called as "the Water Tower of Asia," the TP is one of the most sensitive regions to climate change. The ecosystem and glacier over the TP have been threatened by the warming and moistening (Yang et al., 2014; Yao et al., 2019). In order to make well-planned policies for protecting the Water Tower of Asia and ensure the accuracy of downstream weather simulations, it is of great significance to simulate atmospheric circulation and precipitation over the TP in a reasonable manner.

Despite decades of efforts to improve model performances, reliable simulation of precipitation over the TP remains a challenge. An overall overestimation of summer precipitation over the TP has been found in both general circulation models (Cui et al., 2021; Duan et al., 2013; Lun et al., 2021; Su et al., 2013; Zhu & Yang, 2020) and

regional weather prediction model and climate models (Gao et al., 2015; Gu et al., 2020; Maussion et al., 2014; X. Wang et al., 2021). Several studies had identified the sources of wet bias over the TP, such as the unreasonable water vapor transport owing to relative coarse model resolution and unrealistic terrain representation (Lin et al., 2018; Rahimi et al., 2019; Wang et al., 2020a; Zhou et al., 2019), excessive convective activity resulted from cumulus parameterization scheme (Ou et al., 2020), inaccurate land-atmosphere interactions associated with soil moisture and soil frozen-thawing (Fu et al., 2020; Lv et al., 2020; Yang & Wang, 2019; Yang et al., 2018). Wet bias was also noted in reanalysis data sets (Wang et al., 2018). Convection-permitting models (CPMs), with a horizontal resolution less than 4 km, were constructed to avoid the error-prone convective parameterization and a better representation of complex terrain, small-scale physical and land–atmosphere process, yielding improved precipitation simulations (Prein et al., 2015). Gao et al. (2020) and Zhou et al. (2021) had demonstrated the added value of the CPMs in wind, temperature, and precipitation (including frequency and intensity) simulation over the TP. Li et al. (2020) showed that 4-km CPMs could significantly reduce the wet bias over the TP compared to the 13- and 35-km mesoscale models. Such an improvement was mainly due to turnoff of convective parameterizations and more realistic convective available potential energy (CAPE) simulation. Y. Zhao et al. (2021) showed that CPMs had more reasonable precipitation recycling ratio owing to a better representation of convection, resulting in smaller bias over the TP compared to low-resolution models. Although the magnitude of summer wet bias over the TP had been reduced to a large extent in CPMs, it still remains to be further improved (Li et al., 2021; Zhou et al., 2021). Improved representation of other factors, such as clouds and radiation, should be considered.

Clouds play important roles in the atmospheric system not only for the radiation but also for controlling the formation of precipitation. Strong surface radiative heating, limited moisture and complex terrain interactions, make the TP a region with prominent "popcorn-like" convective clouds in summer (Chen et al., 2015; Li & Zhang, 2016; Xu et al., 2002). The diurnal cycle of cloud fraction is obvious over the TP (Fujinami & Yasunari, 2001) with a peak at 18:00 LST and a minimum at 10:00 LST (Shang et al., 2018). Failure of model to capture these clouds and associated radiation would impact the surface energy budget and thus influence the triggering and development of these convections. It is assumed that cloud and radiation bias and the wet bias might be related. As a result, reliable precipitation over the TP required well simulated cloud and radiation.

In this study, we first implemented the joint-Gaussian probability distribution function (PDF) cloud scheme of Qin et al. (2018) into the WRF model, and then analyzed the effect of cloud and radiation simulation on the wet bias over the TP. The remainder of the article is organized as follows. The default and new cloud schemes are described in Section 2. The data, numerical model setup, and methods are introduced in Section 3. The benefits of the new cloud scheme on the TP precipitation are described in Section 4 with the potential physical mechanisms discussed in Section 5. Conclusions and discussion are in Section 6.

2. Description of Cloud Fraction Scheme

In the present WRF model, the default cloud fraction parameterization scheme is the Xu and Randall (1996) (call as Xu-Randall hereafter) scheme, which calculates the cloud fraction using an empirical formula related to relative humidity and cloud water content. Obviously, the empirical formula in Xu-Randall scheme is unlikely to encompass all natural situations (Tompkins, 2005). For example, the same relative humidity over the TP and eastern China corresponds to rather different cloud fractions (Wang, Zeng, et al., 2020), and it is difficult to reflect this difference using the Xu-Randall scheme. More importantly, Xu-Randall scheme is just a diagnostic cloud fraction scheme and does not consider subgrid condensation. However, the scale of the "popcorn-like" cloud over the TP is less than 1 km, which cannot be resolved even in CPMs. Both cloud fraction and subgrid condensation may directly affect the earth's energy budget by modulating both longwave and shortwave radiation.

As a widely used shortwave radiation scheme in WRF model, the Dudhia scheme, which is used in this study, is a simple shortwave parametrization that considers the effects of solar zenith angle, albedo and absorption of clouds (including rain, snow and graupel particles), and clear-sky scattering and water vapor absorption (Dudhia, 1989). Extinction by other molecules (such as aerosols, ozone) are implicitly included in an empirical scattering parameter (Ruiz-Arias et al., 2013). The albedo and absorption of clouds is calculated from tabulated functions related to the vertically integrated liquid and ice water path. Thus, the subgrid condensation directly affects the shortwave radiation. The longwave radiation scheme used is the RRTM scheme (Mlawer et al., 1997), which uses a look-up table method to calculate longwave radiative transfer of 16 spectral bands in each cloud layer. The longwave

radiative transfer is accomplished by combining gaseous (such as ozone, water vapor, carbon dioxide) and cloud optical thickness, which is related to the cloud water and cloud ice. Thus, the subgrid condensation also directly affects the longwave radiation in RRTM scheme. Therefore, neglecting the subgrid condensation, the Xu-Randall scheme could not capture the impact of "popcorn-like" clouds on radiation over the TP.

Statistical cloud fraction schemes assume a subgrid-scale PDF of potential temperature and total water mixing ratio to calculate the condensation and cloud fraction (Mellor, 1977; Olson et al., 2019a, 2019b; Sommeria & Deardorff, 1977). This scheme takes into account the subgrid impacts of dynamic and thermodynamical conditions. That is, subgrid condensation would occur even if the grid box average relative humidity is below 100%. Application of a PDF cloud scheme in the NCAR Community Atmosphere Model (CAM5) improved the simulation of marine low cloud and alleviated double Intertropical Convergence Zone (ITCZ) problem (Qin & Lin, 2018; Qin et al., 2018). In this study, we implement the Gaussian PDF cloud scheme of Qin et al. (2018) (called as GS-PDF hereafter) into the WRF model with subgrid-scale variance diagnosed from the UW boundary layer turbulence scheme and UW shallow convection scheme in WRF.

The GS-PDF cloud scheme has two basic variables: the total water specific humidity (q_t) and the liquid water potential temperature (θ_l). The scheme assumes that the probability distribution of both q_w and θ_l are Gaussian distributed around their grid mean values. In addition, we made the following modifications.

First, considering prominent mixed-phase clouds over the TP due to its high altitude, we include cloud ice (q_i) into the total water specific humidity (q_t) and the liquid water potential temperature (θ_l) following Cusack et al. (1999) as

$$q_t = q_v + q_c + q_i \tag{1}$$

$$\theta_l = \theta - \frac{L_v \theta}{c_p T} q_c - \frac{(L_v + L_s)\theta}{c_p T} q_i \tag{2}$$

where q_v, q_c, and q_i are the specific humidity of water vapor, cloud water and cloud ice, respectively. θ is the potential temperature, T is the absolute temperature, c_p is the specific heat capacity at constant pressure, L_v and L_s is the latent heat of vapourization and fusion, respectively. The saturation vapor pressure over water and ice is calculated using Murray (1967) method.

Second, the subgrid condensation is simply partitioned into q_c and q_i according to the linear approximation of Hobbs et al. (1974):

$$W_{\text{water}} = \text{MAX}\left(0, \text{MIN}\left(1, \frac{T - 254}{15}\right)\right) \tag{3}$$

$$W_{\text{ice}} = 1 - W_{\text{water}} \tag{4}$$

Then

$$q_c = R * Q * W_{\text{water}} \tag{5}$$

$$q_i = R * Q * W_{\text{ice}} \tag{6}$$

where W_{water} and W_{ice} are the weight coefficients of cloud water and cloud ice, respectively. T is the air temperature (units: K). R is the cloud fraction and Q is the subgrid cloud condensation determined by the PDF scheme. The subgrid condensation q_c and q_i are added to their respective preexisting resolved scale components for the radiation calculation, and the subgrid condensation q_c and q_i have not been passed to cloud microphysics for resolved scale moisture conservation as Olson et al. (2019a).

3. Simulation Setup and Evaluation Data

3.1. Simulation Setup

The WRF-ARW version 4.2.1(Skamarock et al., 2019), a fully compressible, non-hydrostatic model, is used in this study. The model has 50 uneven vertical levels with the model top at 50 hPa, and the center of the model domain locates at (32°N, 83°E) with a grid spacing of 0.1° (approximately 11 km) and 540 × 280 horizontal grid points. Both the initial and lateral boundary conditions were derived from ERA5 (Hersbach et al., 2020). WRF

Table 1
Summary of Station Information in This Study

Number	Station_Name	Latitude (°N)	Longitude (°E)	Altitude (m)
1	Lhasa Tibet	29.67	91.13	3,649
2	Nagqu Tibet	31.48	92.07	4,508
3	Garze Sichuan	31.62	100.00	3,394
4	Yushu Qinghai	33.00	96.96	3,718
5	Hongyuan Sichuan	32.80	102.55	3,493
6	Seng-ge Kambab Tibet	32.50	80.08	4,281
7	Qamdo Tibet	31.15	97.17	3,309
8	Xining Qinghai	36.73	101.75	2,297
9	Gangcha Qinghai	37.33	100.13	3,302
10	Golmud Qinghai	36.41	94.9	2,808
11	Ma Qin Qinghai	34.46	100.25	3,719

Note. Station 1–7 have hourly DSSR and 6 hourly (1200 LST and 1800 LST) sounding profile observations. Station 8–11 only have hourly DSSR observations.

simulation started from 1 to 31 July 2016 using a daily re-initialization strategy (Dong et al., 2018; D. Zhao et al., 2021). Specifically, simulations for each day were conducted by integrating the model for 36 hr starting at 1200 UTC on the previous day. The first 12 hr were discarded as model spin-up and the remaining 24 hr were stitched together to have a full month output.

As suggested by Lv et al. (2020), new Thompson microphysics scheme (Thompson et al., 2008), and the unified Noah land-surface model (Chen & Dudhia, 2001) are used in this study. Following Zhou et al. (2021), we use RRTM (Rapid Radiative Transfer Model) model (Mlawer et al., 1997) for longwave and Dudhia scheme (Dudhia, 1989) for shortwave radiation calculations. UW shallow convection and its corresponding UW planetary boundary layer (PBL) scheme (Bretherton & Park, 2009) are used here because shallow convection is important for the low cloud formation by transporting heat, moisture and momentum from boundary layer to the free atmosphere. Ou et al. (2020) demonstrated that simulation of summer precipitation without a cumulus parameterization scheme performs better than those with a cumulus parameterization at the gray-zone grid space over the TP. Therefore, the deep convection parameterization was turned off. Other model setup includes the Eta surface layer scheme (Janjić, 1994) and the 21-class MODIS land-use data (Friedl et al., 2010). As there are more than 1,000 lakes with area greater than 1 km^2 over the TP (Lazhu et al., 2021; Zhang et al., 2019), the CLM 4.5 lake model (Gu et al., 2015; Subin et al., 2012) is used in this study. The Turbulent Orographic Form Drag (TOFD) parameterization scheme (Beljaars et al., 2004; Zhou et al., 2018) is also used to describe the subgrid-scale orographic impacts.

Two groups of simulations are conducted, one with the GS-PDF cloud fraction scheme and the other using the Xu-Randall scheme. Both simulations used the same setup and configurations described above except the cloud fraction scheme.

3.2. Surface Observations

Surface observations, including hourly precipitation, 2-m temperature (T2) and 6-hourly radiosonde profiles over the TP from 1 to 31 July in 2016 are acquired from the China Integrated Meteorological Information Service System (CIMISS). These data have passed quality control measures (Shen & Xiong, 2016; Sun et al., 2020; Zhao et al., 2017) with unreliable observations set as missing values. There are 847 precipitation and 588 T2 observation stations used in this study with their missing ratios less than15% according to Li (2018). Seven stations have both 1200 LST (0600 UTC) and 1800 LST (1200 UTC) radiosonde profiles over the TP. The corresponding ground-based hourly downward surface shortwave radiation (DSSR) data from 11 stations are obtained from China Meteorological Administration (CMA) (Shi et al., 2008; Tang et al., 2011, 2013). Locations of these stations are summarized in Table 1 and Figure 1.

3.3. Height Correction for Simulated 2-m Temperature

Given the complex terrain over the TP, height between simulations and real terrain might differ significantly. The temperature height correction method of Sheridan et al. (2010) is conducted in this study following D. Zhao et al. (2021). Specifically, for a given station, we use the nearest model grid if its model height discrepancy was less than 25 m. Otherwise, we select the point with the smallest height discrepancy in the surrounding 9 nearest grid points. After the model grid point is selected, the height correction is applied as $T_a = T_m + \gamma(h_m - h_a)$, where T_a is the corrected simulated T2, T_m, h_m are the simulated T2 and terrain height of selected grid point, h_a is the terrain height of station observations. γ is the local value of lapse rate calculated as the linear regression coefficient between the simulated T2 and height variations within the 8 × 8 grid points nearest to that station.

3.4. The Surface Energy Budget

A surface energy budget was conducted following previous studies (Chen et al., 2019; Oehri et al., 2022; Sellers et al., 1997). The surface energy budget consists of the most relevant components:

$$R_n = \mathrm{NSW} + \mathrm{NLW} = \mathrm{SH} + \mathrm{LH} - \mathrm{GH} \quad (7)$$

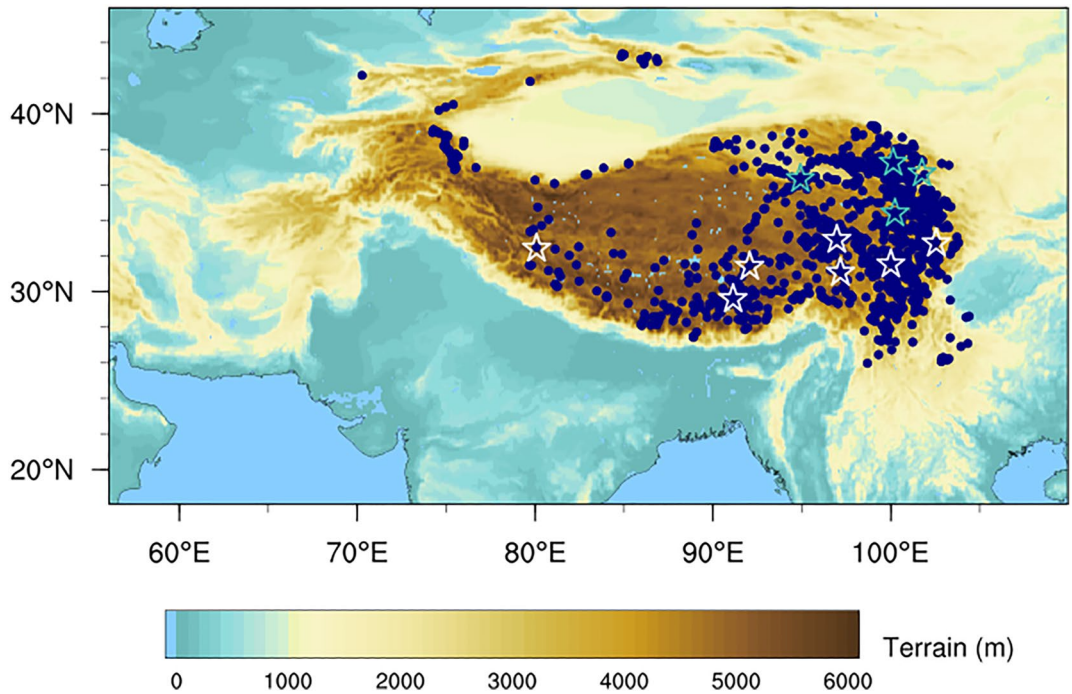

Figure 1. The domain configuration and topography over the Tibetan Plateau and adjacent areas in Weather Research and Forecasting (WRF) simulation. Blue solid dots denote the locations of rainfall gauge stations. Seven white pentagrams indicate the stations with the hourly DSSR and 6 hourly (1200 LST and 1800 LST) sounding profile observations. Four cyan pentagrams indicate the stations only with the hourly DSSR observations.

where R_n is the net radiative flux absorbed by the earth's surface, balanced by sensible heat flux (SH), latent heat flux (LH), and ground heat flux (GH). The net radiative flux (R_n = NSW + NLW) is the sum of the net shortwave radiation flux (NSW) and the net longwave radiation flux (NLW). The net shortwave radiation flux (NSW = $(1 - albedo) * \mathrm{DSSR}$) is the downward shortwave radiation reached earth's surface minus the shortwave radiation reflected upward from the surface. The net longwave radiation flux (NLW = GLW $- \varepsilon\delta T^4$) is the downward ground surface longwave radiation emitted by the overlying atmosphere (GLW) minus the longwave radiation emitted by the earth's surface ($\varepsilon\delta T^4$). *albedo* is the surface albedo, ε is the surface emissivity, T is the surface skin temperature (units: K), δ is the Stefan-Boltzmann constant. SH, LH, and GH are positive upward.

4. Improved Precipitation Simulation

The daily average precipitation in July (Figure 2a) over the TP gradually decreases from southeast to northwest. The nearest grid simulated daily average precipitation are compared with observations in Figures 2b and 2c. The average precipitation bias of all stations during July 2016 over the TP is 0.58 mm/day with a root mean square error (RMSE) of 3.30 mm/day in Xu-Randall (Figure 2b). By contrast, the wet bias is reduced substantially to 0.06 mm/day with the RMSE of 3.03 mm/day using the new cloud scheme (Figure 2c).

The wet bias is prominent in the central eastern and southern part of the TP with several stations showing a wet bias greater than 3 mm/day (Figure 2). The wet bias and RMSE are reduced from 1.22 to 2.32 mm/day in the central eastern (32°N−36°N, 98.5°E−103.5°E, hereafter "east area") in Xu-Randall to 0.60 and 1.77 mm/day in GS-PDF. The wet bias and RMSE in central southern (27°N−33°N, 90°E−96°E, hereafter "south area") in Xu-Randall are 0.63 and 2.23 mm/day, which are reduced to 0.15 and 2.13 mm/day in GS-PDF. Wet biases persist along the southern plateau margin in both experiments, and this might be related to overestimated moisture transport due to the coarse model resolution as suggested by Lin et al. (2018) and Wang et al. (2020a).

Figure 3 shows observed and simulated diurnal cycle of average precipitation in the east and south areas during July 2016. The observed precipitation peaks in the late afternoon and early evening in the east area, captured by the model reasonably well (Figure 3a). Xu-Randall significantly overestimates the amount of precipitation in the

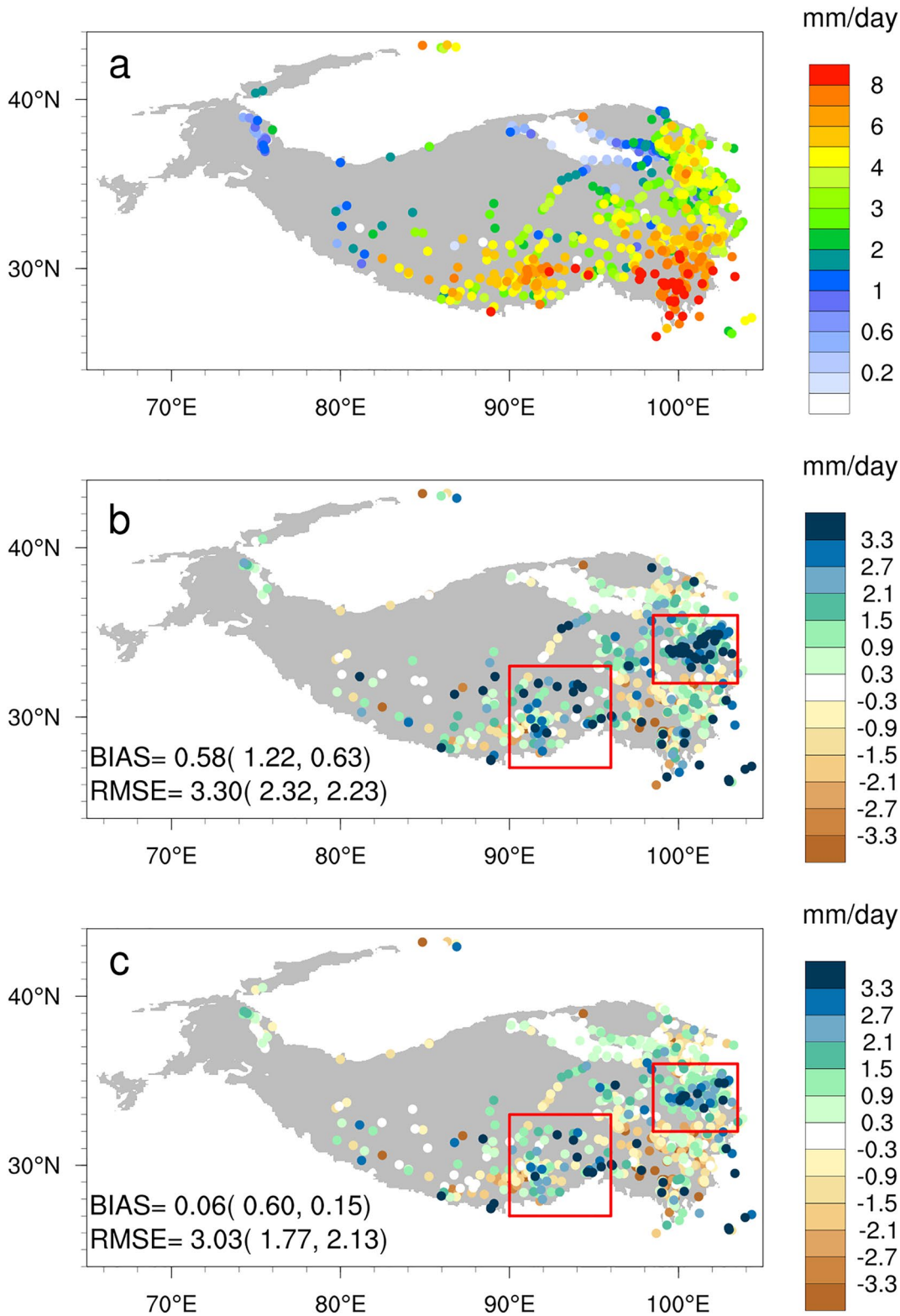

Figure 2. Geographical observed daily precipitation (a, units: mm/day) and biases in Xu-Randall (b) and GS-PDF (c) simulations during July 2016. The red boxes represent two areas with large wet bias. Values outside brackets represent the BIAS and RMSE of all stations, the first (second) values in brackets represent the BIAS and RMSE in east (south) red box.

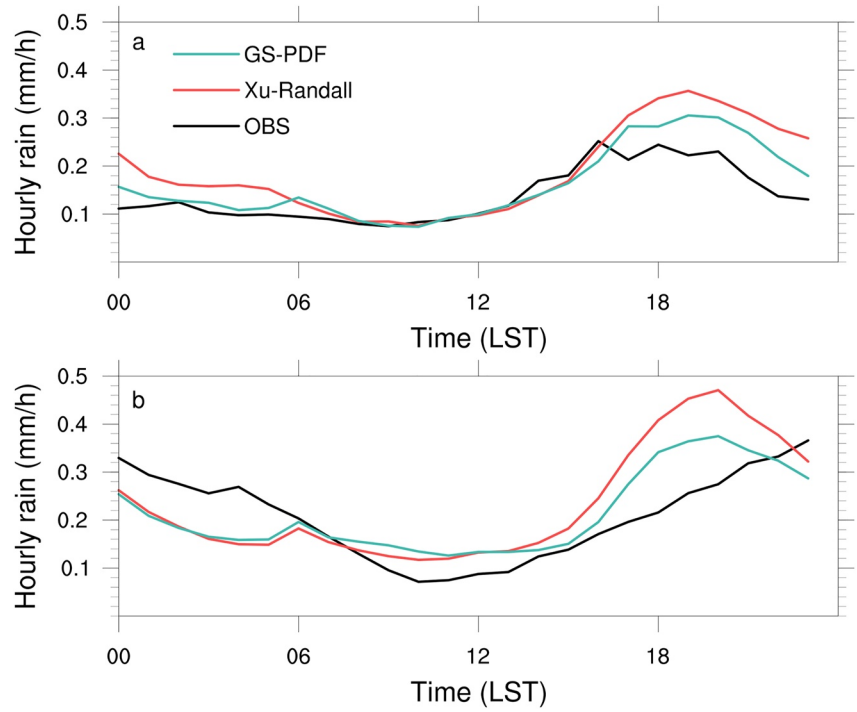

Figure 3. The observed and simulated diurnal cycle of average precipitation (units: mm/h) in east (a) and south (b) red box in Figure 2 during July 2016 over the Tibetan Plateau.

late afternoon, while GS-PDF reduces the overestimate by about an half (Figure 3a). In the south area, observed precipitation peaks around midnight with a minimum around 10:00 LST, but the simulated precipitation peaks much earlier around 20:00 LST (Figure 3b). This may be related to the unresolved local valley winds (Barros et al., 2000; Kuo & Qian, 1981; Ye, 1981; Zhao et al., 2022) and moisture transport (Liu et al., 2022). In terms of precipitation amount, the large overestimation in Xu-Randall is reduced in GS-PDF. Overall, the GS-PDF cloud scheme effectively improve precipitation simulation with an obvious reduction of precipitation in the late afternoon and early evening. The following analysis will focus on the mechanisms for such an improvement.

5. Possible Mechanisms

5.1. Alleviated DSSR Overestimation

Figures 4a and 4b shows simulated diurnal cycle of weighted total cloud water (TCW) mixing ratio during July 2016 over the TP in two experiments. Based on Dudhia shortwave radiation scheme, the weighted TCW can be written as

$$\mathrm{TCW} = q_c + 0.1 * q_i + 0.05 * q_r + 0.02 * q_s + 0.05 * q_g \tag{8}$$

where q_c, q_i, q_r, q_s, q_g are the mixing ratio of cloud water, cloud ice, rain, show and graupel particles, respectively. As shown in Figure 4a, the weighted TCW is mainly distributed in the middle and lower troposphere, with the 0.005 g/kg contour rising from about 400 hPa in the late morning to approximately 300 hPa in the late afternoon in Xu-Randall. This rise in afternoon is also obvious in GS-PDF (Figure 4b), probably related to the prevalent afternoon convection simulated. The weighted TCW in GS-PDF is about 20% greater than that in Xu-Randall (Figure 4c). The different TCW between GS-PDF and Xu-Randall principally results from the additional cloud water (or ice) formed by subgrid condensation (Figure 4d).

The TCW could directly impact the downward surface shortwave and longwave radiation (Letu et al., 2020). The simulated DSSR diurnal cycle during July 2016 is compared with surface observations over the TP (Figure 5). The DSSR of Xu-Randall is greater than the ground observations, with the largest bias reaching 100 W/m^2 near noon. The DSSR overestimation in the WRF model has been documented in several previous studies (Ruiz-Arias

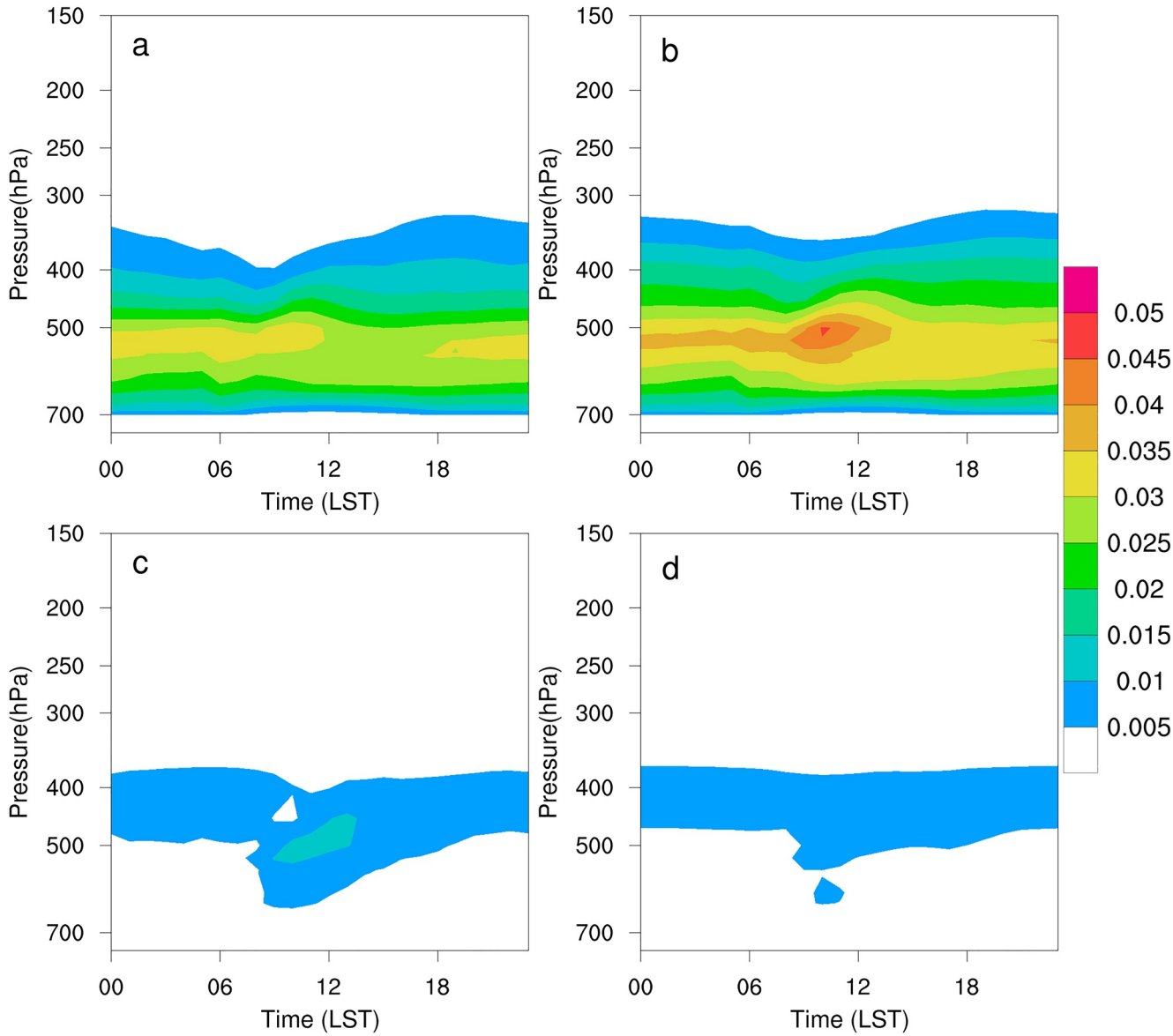

Figure 4. The simulated diurnal cycle of weighted total cloud water mixing ratio (units: g/kg) during July 2016 over the Tibetan Plateau in Xu-Randall (a), GS-PDF (b) simulations and their difference (GS-PDF minus Xu-Randall, (c), and additional cloud water formed by subgrid condensation in GS-PDF scheme (d), which is already included in panel (b).

et al., 2016; Thompson et al., 2016; Yun et al., 2020). In contrast, the overestimate is significantly reduced with a slight underestimate (~10–15 W/m^2) near noon in the GS-PDF. The much-reduced DSSR bias is related to the increased albedo and absorption of shortwave radiation by the increased TCW. The simulated GLW in GS-PDF is about 15 W/m^2 larger than that in Xu-Randall in the morning, also due to the increased TCW (not shown).

5.2. Reduced Latent and Sensible Heat Flux

To explore the impact of simulated DSSR on the atmosphere over the TP, the surface heat budget described in Section 3.4 is presented here. Similar to the diurnal cycle of DSSR shown in Figure 5, all heat flux terms in Xu-Randall are greater than those in GS-PDF. The highest NSW at noon in Xu-Randall is above 600 W/m^2, about 70% of the total DSSR due to ground reflection (Figure 6a). Affected by the incoming solar radiation, the surface skin temperature gradually increases, and the NLW reaches its maximum of about 110 W/m^2 at noon (Figure 6b). Most of the solar radiation received by the ground is transmitted to the atmosphere in the form of sensible heat and latent heat. The SH peak is ~210 W/m^2 (Figure 6c), greater than the LH peak of 155 W/m^2 (Figure 6d).

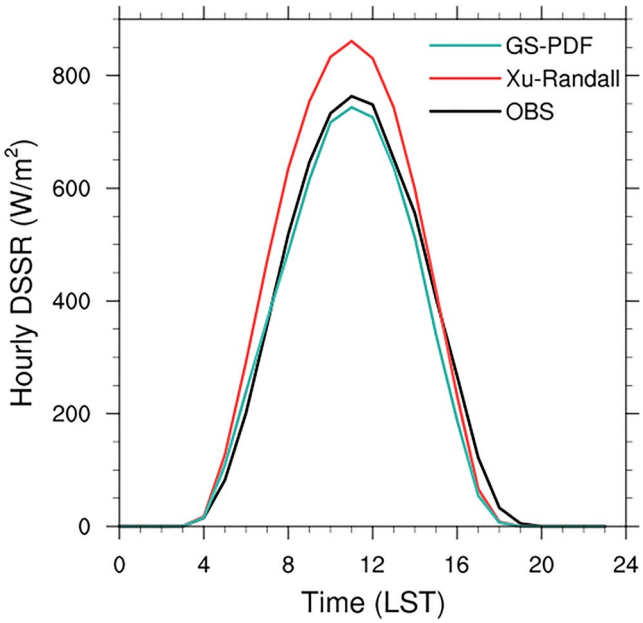

Figure 5. The observed and simulated diurnal cycle of average DSSR during July 2016 at 11 stations over the Tibetan Plateau.

Ground heat flux is ~105 W/m^2 during daytime (Figure 6e). In GS-PDF, the reduced DSSR would reduce surface skin temperature and canopy transpiration (Chen & Dudhia, 2001), lead to reduced surface longwave emission, SH and LH. The significant decreased NLW (upward) in GS-PDF in the morning (Figure 6b) is due to the increased GLW (downward) and decreased surface longwave emission (upward). Reduction of SH (about 27.80 W/m^2) is larger than LH (about 21.80 W/m^2) at noon (Figures 6c and 6d).

The sensible heat flux heats the overlying air column and raises the near-surface atmospheric temperature (Sellers et al., 1997). Although advection and precipitation also impact air temperature (Mazhar et al., 2021; D. Zhao et al., 2021), SH strongly impacts atmospheric temperature in the PBL. Larger SH in the afternoon in Xu-Randall would increase low-level atmospheric temperature. Given the land-cover types and land surface process are the same in both experiments, more evaporation and transpiration in Xu-Randall would moisten the boundary layer.

5.3. Reduced Atmospheric Instability

The influence of different SH on low-level atmospheric temperature is mirrored in the T2 distribution. Figure 7a shows the geographical distribution of averaged T2 in Xu-Randall at 1500 LST during July 2016. Generally, the geographic distribution of T2 is elevation-dependent. T2 is lower in the afternoon in the western part and Himalayas area, followed by the central and eastern plateau. The highest T2 occurs in the Qaidam Basin. The simulated T2 in GS-PDF (Figure 7b) is lower than that of Xu-Randall over most of the TP by about 1.0°C with a few regions showing slightly higher values. Different LH can be partially mirrored in the specific humidity distribution. Low-level specific humidity can be strongly influenced by inherent complexity of land-atmosphere interactions. 500-hPa (roughly represents the boundary layer over the TP) specific humidity in Xu-Randall at 1500 LST during July 2016 decreases from south to north (Figure 7c), similar to the aridity index pattern over the TP (not shown). GS-PDF has smaller (greater) 500 hPa specific humidity than Xu-Randall in areas approximately east (west) of 90°E.

CAPE (calculated from the surface along a pseudoadiabat) at 1500 LST decreased from southeastern to northwestern TP in Xu-Randall (Figure 7e), related to the distribution of surface temperature and specific humidity (Figures 7a and 7c). The differences of CAPE between GS-PDF and Xu-Randall (Figure 7f) mostly reflect the differences in T2. In the eastern and southern TP, CAPE is significantly reduced in GS-PDF due to obviously colder T2. However, in the western TP, CAPE is larger in GS-PDF due to larger T2 and specific humidity.

Figure 8 compares simulated T2 at 1500 LST with surface observations. T2 was overestimated in most stations with the mean bias (RMSE) of 0.46°C (1.93°C) in Xu-Randall (Figure 8a), but reduced to −0.36°C (1.82°C) in GS-PDF (Figure 8b). In the two regions with large wet bias in Xu-Randall (Figure 2b), T2 bias (RMSE) is 0.15°C (1.24°C) and 0.40°C (2.18°C) in the east and south region. With reduced DSSR, T2 is significantly reduced over these two regions, with most stations having a cold bias in the east (−0.78°C) and south (−0.64°C) region in GS-PDF. This would influence simulated CAPE and thus afternoon convection and precipitation accordingly.

Simulated CAPE is compared with observed at 7 sounding stations at 1200 and 1800 LST (Figure 9). The CAPE over the TP is very small in the early morning and increased rapidly before noon and then gradually decreased in the afternoon. At Lhasa, Nagqu and Garze stations (Figures 9a–9c), Xu-Randall overestimates the CAPE at noon, while the overestimation is alleviated in GS-PDF, in better agreement with observed. At Yushu and Hongyuan stations (Figures 9d and 9e), the simulated CAPE is close to observed. But both simulations did not capture the large CAPE value at1800 LST at Hongyuan station. At Seng-ge Kambab and Qamdo stations (Figures 9f and 9g), the simulated CAPE is smaller than observed, may be related to the altitude difference between the nearest model grid and stations. The altitude of Seng-ge Kambab and Qamdo Station is 4281 and 3309 m, but the altitude of the grid point closest is 4412 and 3936 m, respectively. Nevertheless, the notable feature is the reduced CAPE in GS-PDF at all stations and times except at Seng-ge Kambab. This is probably related to the reduced DSSR and T2 as discussed above.

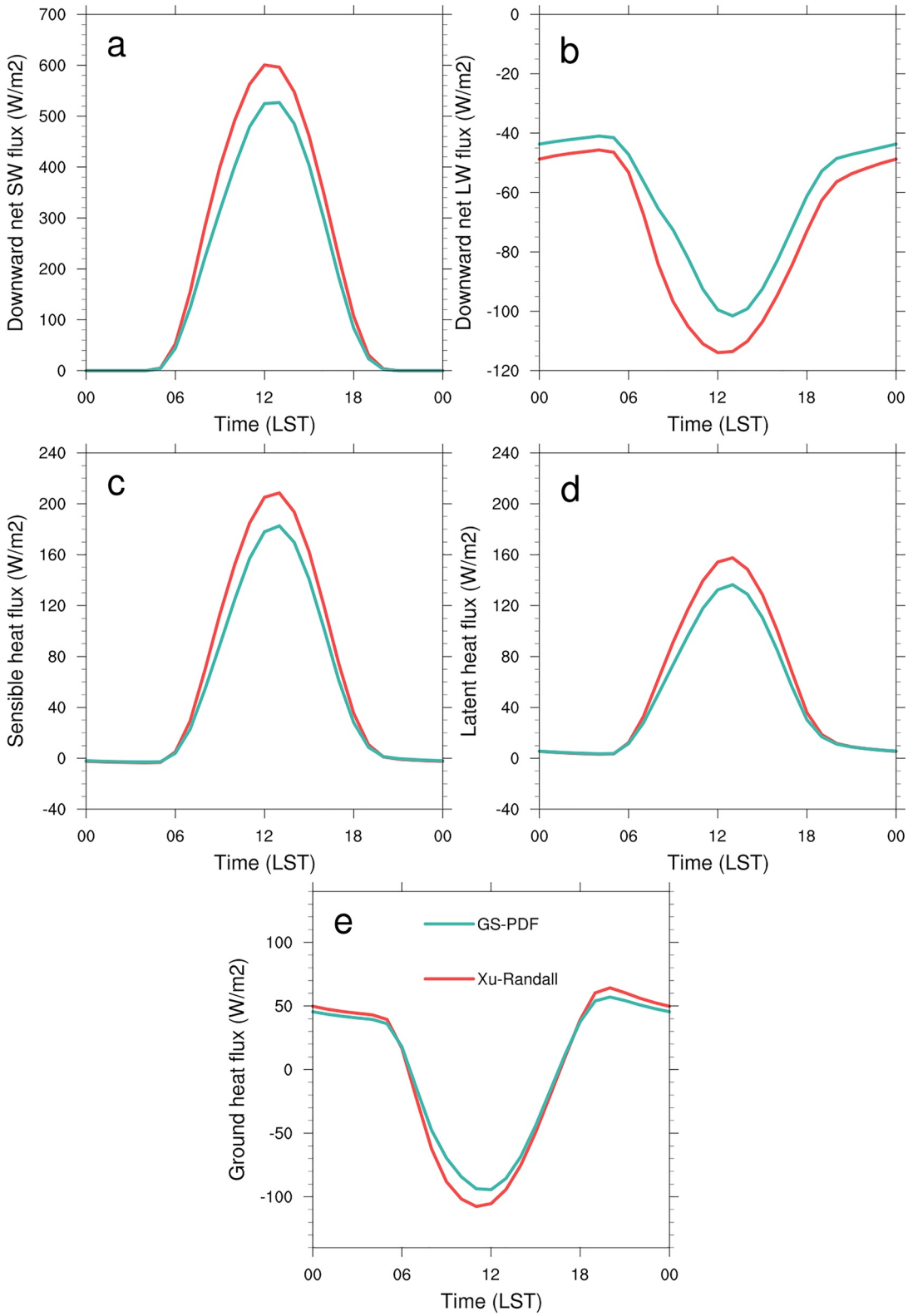

Figure 6. The diurnal cycle of downward net shortwave flux (a), downward net longwave flux (b), sensible heat flux (c), latent heat flux (d) and ground heat flux (e) in the two simulations.

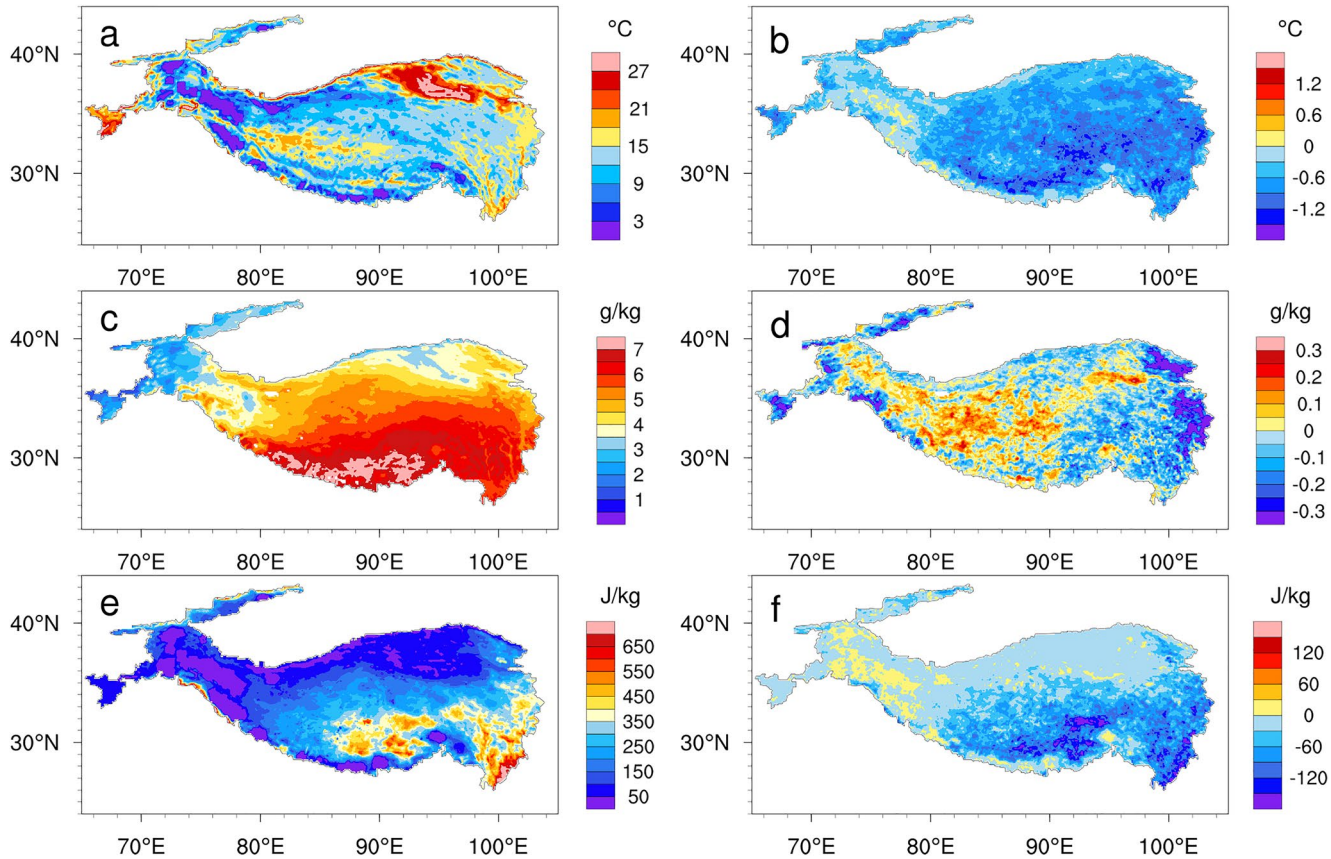

Figure 7. Geographical average T2 (a, units: °C), 500 hPa specific humidity (c, units: k/kg) and CAPE (e, units: J/kg) in Xu-Randall simulation at 1500 LST during July 2016, and the difference of T2 (b), specific humidity (d) and CAPE (f) between GS-PDF simulation and Xu-Randall simulation.

5.4. Dependence of Wet Bias on Atmospheric Instability

In general, larger simulated CAPE might lead to more frequent convection and thus overestimated precipitation. To explore a possible connection between CAPE and rainfall, we plot the CAPE bias at 12 LST and the subsequent 6-hr average rainfall bias at 5 representative stations (2 stations with large altitude bias were excluded) in Xu-Randall and GS-PDF (Figure 10). A strong correlation ($r^2 = 0.65, p < 0.005$) between the two biases is evident and robust in both simulations. This indicates that the overestimated CAPE could lead to wet bias. With reduced CAPE bias in GS-PDF, it is expected that the rainfall bias will be reduced too. Note that both rainfall frequency and intensity are reduced in GS-PDF (Figures S1 and S2 in Supporting Information S1).

In conclusion, the mechanism for alleviated wet bias over the TP in this study can be summarized as a cloud radiation-low level temperature/moisture-CAPE-precipitation loop in Figure 11. Compared with Xu-Randall scheme, the subgrid condensation in GS-PDF increased the water content of middle and low clouds (Figure 4), which alleviated the DSSR overestimation (Figure 5) and reduced the sensible and latent heat flux (Figure 6). Reduced sensible and latent heat flux lowered the low-level temperature and moisture, lead to reduced atmospheric instability (Figure 7), which result in reduced rainfall over the TP (Figure 2). In addition, overestimated DSSR also lead to larger rainfall recycling rate (i.e., the proportion of precipitation formed by the condensation of local evaporative water vapor to the total precipitation (Brubaker et al., 1993; Yang et al., 2022)) in Xu-Randall (not shown), demonstrating the close connection between local surface energy budget and hydrological cycle over the TP (Allen & Ingram, 2002; Wu et al., 2013).

6. Discussion and Conclusions

Despite the ongoing efforts to alleviate the wet bias over TP, further improvements are still needed. Considering the strength of the hydrological cycle is closely related to the surface energy budget and prevailing "popcorn-like" clouds over the TP in summer would impact surface radiation, in this study, the statistical cloud fraction and

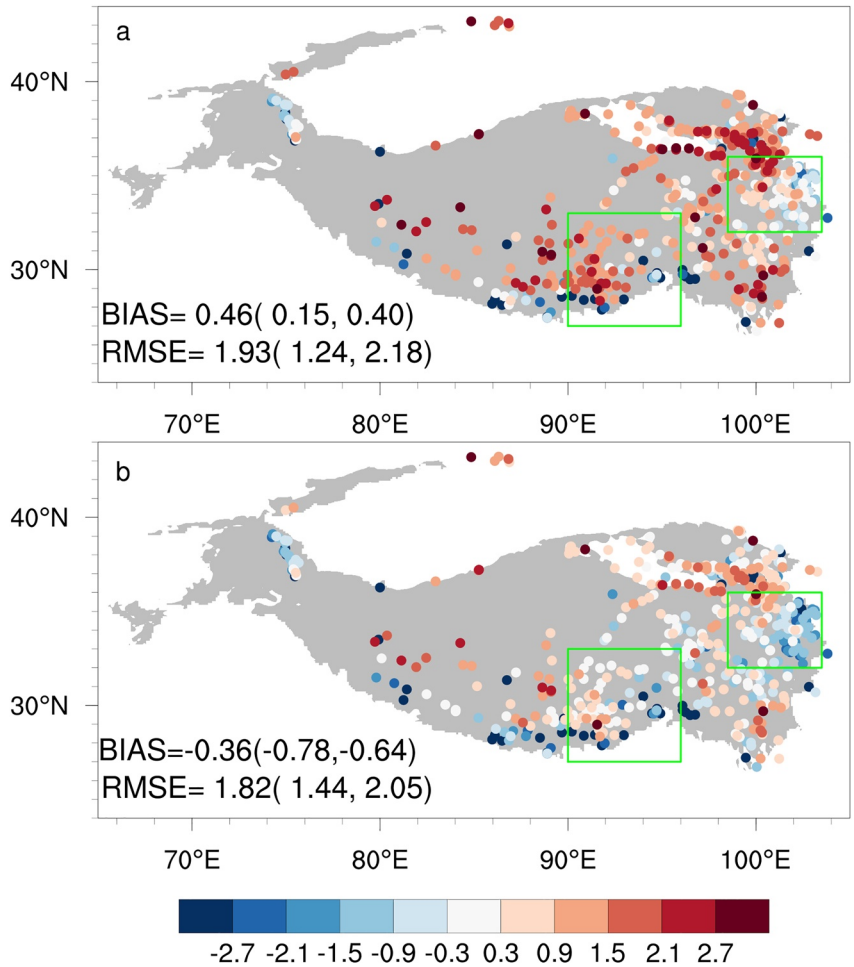

Figure 8. Geographical biases of average T2 (a–d, units: °C) at 1500 LST in Xu-Randall (a) and GS-PDF (b) simulations during July 2016. The green boxes represent two areas with large wet bias in Figure 2. Values outside brackets represent the BIAS and RMSE of all stations, the first (second) values in brackets represent the BIAS and RMSE in east (south) green box.

subgrid condensation scheme (GS-PDF scheme) of Qin et al. (2018) is implemented and tested in the WRF model. In contrast to the default Xu-Randall scheme, the GS-PDF scheme effectively mitigates the wet bias over TP. The diurnal cycle of precipitation in the two regions with prominent wet bias shows that the GS-PDF scheme clearly suppresses the convective precipitation in the late afternoon and early evening.

This study then explores the physical mechanisms responsible for the alleviation of wet bias. Considering the subgrid variation of temperature and humidity, the GS-PDF scheme better captures clouds over the TP with more mid-low cloud water (ice) than the Xu-Randall scheme. The default Xu-Randall scheme in WRF tends to overestimate the DSSR, surface temperature, low-level humidity, CAPE, and convective precipitation in summer over the TP. Increased mid-low cloud water in the GS-PDF scheme reduced simulated DSSR, improved surface temperatures and atmospheric instabilities, leading to alleviated wet bias over the TP.

Although the new cloud fraction scheme had been proved to be effective in reducing the wet bias, further explorations are warranted. The statistical cloud scheme only works with the UW boundary layer and shallow convection schemes at present. A more flexible scheme considering subgrid perturbation of temperature and humidity is needed in the future. The GS-PDF scheme may slightly over-reduce the NSW, resulting in cooler temperatures, which should be further explored. Similar to previous studies (Li et al., 2021; Liu et al., 2022; Ou et al., 2020), the simulated precipitation peaks in the southern TP are still earlier than gauge observation in this study. The coarse-resolution may be one of the reasons, but other avenues for the wrong precipitation diurnal peak need to be explored.

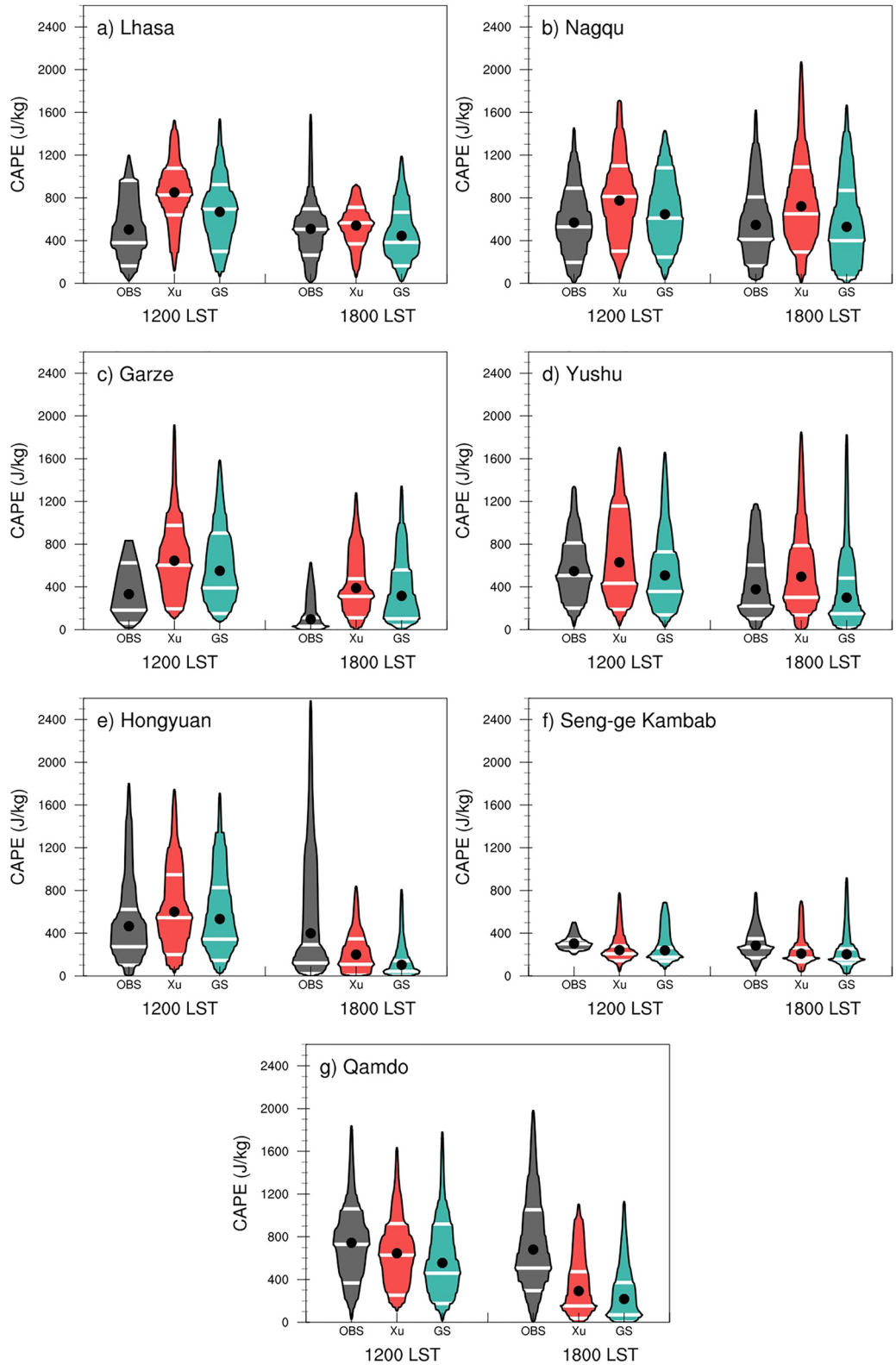

Figure 9. The CAPE at 1200 and 1800 LST of observation (gray box) and WRF simulation (red and green boxes for Xu-Randall and GS-PDF simulations, respectively) at 7 meteorological stations over the Tibetan Plateau. The black solid dots in the box plot indicate mean values. The white short dashes in the box plot indicate the 25th, 50th, and 75th percentiles from the bottom up.

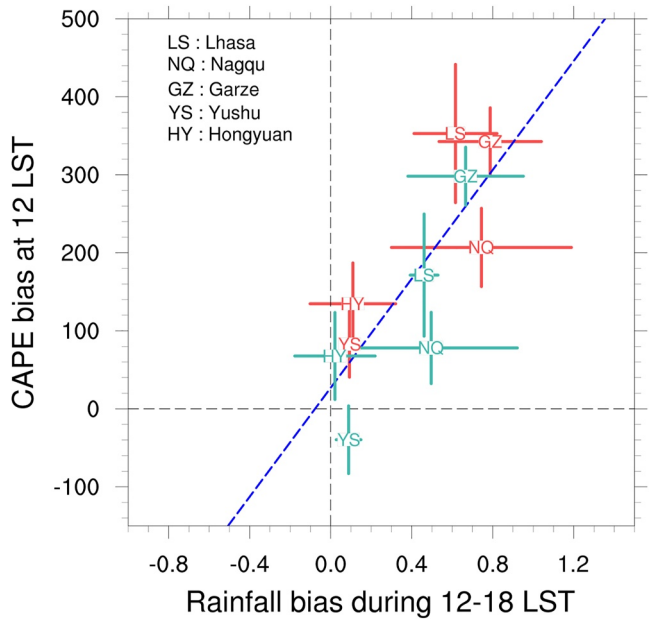

Figure 10. The relationship between CAPE bias (units: J/kg) at 12 LST at 5 representative stations and the subsequent 6 hr' average rainfall bias (units: mm/h) in an area of a 100 km radius around the representative stations in Xu-Randall (red) and GS-PDF (green) simulations during July in 2016.

Other model deficiencies, such as microphysical parameterizations (Caldwell et al., 2009; Gao et al., 2016; Xu et al., 2020), the deep or shallow convection schemes (Li et al., 2021; Ou et al., 2020), water vapor transport (Y. Zhao et al., 2021) and the misrepresented land-atmosphere interactions associated with soil physical properties (including soil moisture, temperature and soil type classification) and soil frozen-thawing (Fu et al., 2020; Lv et al., 2020; Yang & Wang, 2019; Yang et al., 2018), might also be able to initiate or amplify the wet bias. In order to obtain a more realistic simulation of cloud and precipitation over the TP, all these should be carefully analyzed to better understand and simulate the hydrological cycle over the TP.

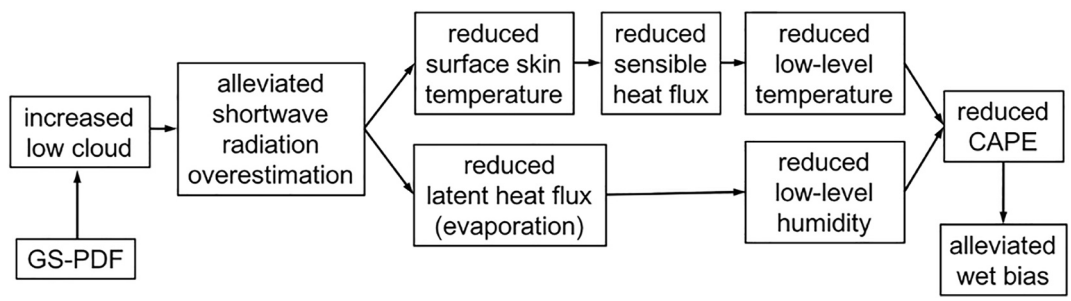

Figure 11. A schematic of physical mechanisms for the alleviated wet bias over the Tibetan Plateau.

Conflict of Interest

The authors declare no conflicts of interest relevant to this study.

Data Availability Statement

We gratefully acknowledge all the data centers for providing public access to the data products used in this study. The ERA5 data can be downloaded from the website https://cds.climate.copernicus.eu/. Meteorological station observations are obtained from the China Meteorological Data Sharing Service System http://data.cma.cn. The source code of the scheme is available at https://doi.org/10.6084/m9.figshare.21972944.

Acknowledgments
This work was supported by the Second Tibetan Plateau Scientific Expedition and Research Program (2019QZKK0206) and the National Natural Science Foundation of China (41975127).

References

Allen, M. R., & Ingram, W. J. (2002). Constraints on future changes in climate and the hydrologic cycle. *Nature*, *419*(6903), 224–232. https://doi.org/10.1038/nature01092

Barros, A. P., Joshi, M., Putkonen, J., & Burbank, D. W. (2000). A study of the 1999 monsoon rainfall in a mountainous region in central Nepal using TRMM products and rain gauge observations. *Geophysical Research Letters*, *27*(22), 3683–3686. https://doi.org/10.1029/2000gl011827

Beljaars, A. C. M., Brown, A. R., & Wood, N. (2004). A new parametrization of turbulent orographic form drag. *Quarterly Journal of the Royal Meteorological Society*, *130*(599), 1327–1347. https://doi.org/10.1256/qj.03.73

Bretherton, C. S., & Park, S. (2009). A new moist turbulence parameterization in the community atmosphere model. *Journal of Climate*, *22*(12), 3422–3448. https://doi.org/10.1175/2008jcli2556.1

Brubaker, K. L., Entekhabi, D., & Eagleson, P. S. (1993). Estimation of continental precipitation recycling. *Journal of Climate*, *6*(6), 1077–1089. https://doi.org/10.1175/1520-0442(1993)006<1077:eocpr>2.0.co;2

Caldwell, P., Chin, H. N. S., Bader, D. C., & Bala, G. (2009). Evaluation of a WRF dynamical downscaling simulation over California. *Climatic Change*, *95*(3–4), 499–521. https://doi.org/10.1007/s10584-009-9583-5

Chen, C.-C., Lo, M.-H., Im, E.-S., Yu, J.-Y., Liang, Y.-C., Chen, W.-T., et al. (2019). Thermodynamic and dynamic responses to deforestation in the maritime continent: A modeling study. *Journal of Climate*, *32*(12), 3505–3527. https://doi.org/10.1175/jcli-d-18-0310.1

Chen, F., & Dudhia, J. (2001). Coupling an advanced land surface-hydrology model with the Penn State-NCAR MM5 modeling system. Part I: Model implementation and sensitivity. *Monthly Weather Review*, *129*(4), 569–585. https://doi.org/10.1175/1520-0493(2001)129<0569:caalsh>2.0.co;2

Chen, J., Wu, X., Yin, Y., & Xiao, H. (2015). Characteristics of heat sources and clouds over eastern China and the Tibetan Plateau in boreal summer. *Journal of Climate*, *28*(18), 7279–7296. https://doi.org/10.1175/jcli-d-14-00859.1

Cui, T., Li, C., & Tian, F. (2021). Evaluation of temperature and precipitation simulations in CMIP6 models over the Tibetan Plateau. *Earth and Space Science*, *8*(7), e2020EA001620. https://doi.org/10.1029/2020ea001620

Cusack, S., Edwards, J. M., & Kershaw, R. (1999). Estimating the subgrid variance of saturation, and its parametrization for use in a GCM cloud scheme. *Quarterly Journal of the Royal Meteorological Society*, *125*(560), 3057–3076. https://doi.org/10.1002/qj.49712556013

Dong, W., Lin, Y., Wright, J. S., Xie, Y., Xu, F., Yang, K., et al. (2018). Connections between a late summer snowstorm over the southwestern Tibetan Plateau and a concurrent Indian monsoon low-pressure system. *Journal of Geophysical Research: Atmospheres*, *123*(24), 13676–13691. https://doi.org/10.1029/2018jd029710

Duan, A., Hu, J., & Xiao, Z. (2013). The Tibetan Plateau summer monsoon in the CMIP5 simulations. *Journal of Climate*, *26*(19), 7747–7766. https://doi.org/10.1175/jcli-d-12-00685.1

Dudhia, J. (1989). Numerical study of convection observed during the winter monsoon experiment using a mesoscale two-dimensional model. *Journal of the Atmospheric Sciences*, *46*(20), 3077–3107. https://doi.org/10.1175/1520-0469(1989)046<3077:nsocod>2.0.co;2

Friedl, M. A., Sulla-Menashe, D., Tan, B., Schneider, A., Ramankutty, N., Sibley, A., & Huang, X. (2010). MODIS collection 5 global land cover: Algorithm refinements and characterization of new datasets. *Remote Sensing of Environment*, *114*(1), 168–182. https://doi.org/10.1016/j.rse.2009.08.016

Fu, Y., Ma, Y., Zhong, L., Yang, Y., Guo, X., Wang, C., et al. (2020). Land-surface processes and summer-cloud-precipitation characteristics in the Tibetan Plateau and their effects on downstream weather: A review and perspective. *National Science Review*, *7*(3), 500–515. https://doi.org/10.1093/nsr/nwz226

Fujinami, H., & Yasunari, T. (2001). The seasonal and intraseasonal variability of diurnal cloud activity over the Tibetan Plateau. *Journal of the Meteorological Society of Japan*, *79*(6), 1207–1227. https://doi.org/10.2151/jmsj.79.1207

Gao, W., Sui, C.-H., Fan, J., Hu, Z., & Zhong, L. (2016). A study of cloud microphysics and precipitation over the Tibetan Plateau by radar observations and cloud-resolving model simulations. *Journal of Geophysical Research: Atmospheres*, *121*(22), 13735–13752. https://doi.org/10.1002/2015jd024196

Gao, Y., Chen, F., & Jiang, Y. (2020). Evaluation of a convection-permitting modeling of precipitation over the Tibetan Plateau and its influences on the simulation of snow-cover fractione. *Journal of Hydrometeorology*, *21*(7), 1531–1548. https://doi.org/10.1175/jhm-d-19-0277.1

Gao, Y., Xu, J., & Chen, D. (2015). Evaluation of WRF mesoscale climate simulations over the Tibetan Plateau during 1979-2011. *Journal of Climate*, *28*(7), 2823–2841. https://doi.org/10.1175/jcli-d-14-00300.1

Gu, H., Jin, J., Wu, Y., Ek, M. B., & Subin, Z. M. (2015). Calibration and validation of lake surface temperature simulations with the coupled WRF-lake model. *Climatic Change*, *129*(3), 471–483. https://doi.org/10.1007/s10584-013-0978-y

Gu, H. H., Yu, Z. B., Peltier, W. R., & Wang, X. Y. (2020). Sensitivity studies and comprehensive evaluation of RegCM4.6.1 high-resolution climate simulations over the Tibetan Plateau. *Climate Dynamics*, *54*(7–8), 3781–3801. https://doi.org/10.1007/s00382-020-05205-6

Hersbach, H., Bell, B., Berrisford, P., Hirahara, S., Horanyi, A., Munoz-Sabater, J., et al. (2020). The ERA5 global reanalysis. *Quarterly Journal of the Royal Meteorological Society*, *146*(730), 1999–2049. https://doi.org/10.1002/qj.3803

Hobbs, P. V., Radke, L. F., Weiss, R. R., Atkinson, D. G., Locatelli, J. D., Biswas, K. R., et al. (1974). *The structure of clouds and precipitation over the Cascade Mountains and their modification by artificial seeding (1972–1973). Research Report 8* (p. 181). Department of Atmospheric Sciences, University of Washington.

Janjić, Z. I. (1994). The step-mountain Eta coordinate model: Further developments of the convection, viscous sublayer, and turbulence closure schemes. *Monthly Weather Review*, *122*(5), 927–945. https://doi.org/10.1175/1520-0493(1994)122<0927:tsmecm>2.0.co;2

Kuo, H. L., & Qian, Y. F. (1981). Influence of the Tibetian Plateau on cumulative and diurnal changes of weather and climate in summer. *Monthly Weather Review*, *109*(11), 2337–2356. https://doi.org/10.1175/1520-0493(1981)109<2337:iottpo>2.0.co;2

Lazhu, Yang, K., Hou, J., Wang, J., Lei, Y., Zhu, L., et al. (2021). A new finding on the prevalence of rapid water warming during lake ice melting on the Tibetan Plateau. *Science Bulletin*, *66*(23), 2358–2361. https://doi.org/10.1016/j.scib.2021.07.022

Letu, H., Shi, J., Li, M., Wang, T., Shang, H., Lei, Y., et al. (2020). A review of the estimation of downward surface shortwave radiation based on satellite data: Methods, progress and problems. *Science China Earth Sciences*, *63*(6), 774–789. https://doi.org/10.1007/s11430-019-9589-0

Li, J. (2018). Hourly station-based precipitation characteristics over the Tibetan Plateau. *International Journal of Climatology*, *38*(3), 1560–1570. https://doi.org/10.1002/joc.5281

Li, P., Furtado, K., Zhou, T., Chen, H., & Li, J. (2020). Convection-permitting modelling improves simulated precipitation over the central and eastern Tibetan Plateau. *Quarterly Journal of the Royal Meteorological Society*, *147*(734), 341–362. https://doi.org/10.1002/qj.3921

Li, P. X., Furtado, K., Zhou, T. J., Chen, H. M., & Li, J. (2021). Convection-permitting modelling improves simulated precipitation over the central and eastern Tibetan Plateau. *Quarterly Journal of the Royal Meteorological Society*, *147*(734), 341–362. https://doi.org/10.1002/qj.3921

Li, Y., & Zhang, M. (2016). Cumulus over the Tibetan Plateau in the summer based on CloudSat-CALIPSO data. *Journal of Climate*, *29*(3), 1219–1230. https://doi.org/10.1175/jcli-d-15-0492.1

Lin, C., Chen, D., Yang, K., & Ou, T. (2018). Impact of model resolution on simulating the water vapor transport through the central Himalayas: Implication for models' wet bias over the Tibetan Plateau. *Climate Dynamics*, *51*(9–10), 3195–3207. https://doi.org/10.1007/s00382-018-4074-x

Liu, Y., Lu, M., Yang, H., Duan, A., He, B., Yang, S., & Wu, G. (2020). Land-atmosphere-ocean coupling associated with the Tibetan Plateau and its climate impacts. *National Science Review*, *7*(3), 534–552. https://doi.org/10.1093/nsr/nwaa011

Liu, Z. Y., Gao, Y. H., & Zhang, G. (2022). How well can a convection-permitting-modelling improve the simulation of summer precipitation diurnal cycle over the Tibetan Plateau? *Climate Dynamics*, *58*(11–12), 3121–3138. https://doi.org/10.1007/s00382-021-06090-3

Lun, Y. R., Liu, L., Cheng, L., Li, X. P., Li, H., & Xu, Z. X. (2021). Assessment of GCMs simulation performance for precipitation and temperature from CMIP5 to CMIP6 over the Tibetan Plateau. *International Journal of Climatology*, *41*(7), 3994–4018. https://doi.org/10.1002/joc.7055

Lv, M., Xu, Z., & Yang, Z.-L. (2020). Cloud resolving WRF simulations of precipitation and soil moisture over the central Tibetan Plateau: An assessment of various physics options. *Earth and Space Science*, *7*(2), e2019EA000865. https://doi.org/10.1029/2019ea000865

Maussion, F., Scherer, D., Moelg, T., Collier, E., Curio, J., & Finkelnburg, R. (2014). Precipitation seasonality and variability over the Tibetan Plateau as resolved by the high Asia reanalysis. *Journal of Climate*, *27*(5), 1910–1927. https://doi.org/10.1175/jcli-d-13-00282.1

Mazhar, U., Jin, S. G., Duan, W. T., Bilal, M., Ali, M. A., & Farooq, H. (2021). Spatio-temporal trends of surface energy budget in Tibet from satellite remote sensing observations and reanalysis data. *Remote Sensing*, *13*(2), 256. https://doi.org/10.3390/rs13020256

Mellor, G. L. (1977). The Gaussian cloud model relations. *Journal of the Atmospheric Sciences*, *34*(2), 356–358. https://doi.org/10.1175/1520-0469(1977)034<0356:tgcmr>2.0.co;2

Mlawer, E. J., Taubman, S. J., Brown, P. D., Iacono, M. J., & Clough, S. A. (1997). Radiative transfer for inhomogeneous atmospheres: RRTM, a validated correlated-k model for the longwave. *Journal of Geophysical Research*, *102*(D14), 16663–16682. https://doi.org/10.1029/97jd00237

Murray, F. W. (1967). On the computation of saturation vapor pressure. *Journal of Applied Meteorology and Climatology*, *6*(1), 203–204. https://doi.org/10.1175/1520-0450(1967)006<0203:otcosv>2.0.co;2

Oehri, J., Schaepman-Strub, G., Kim, J.-S., Grysko, R., Kropp, H., Grünberg, I., et al. (2022). Vegetation type is an important predictor of the arctic summer land surface energy budget. *Nature Communications*, *13*(1), 6379. https://doi.org/10.1038/s41467-022-34049-3

Olson, J. B., Kenyon, J. S., Angevine, W. A., Brown, J. M., Pagowski, M., & Sušelj, K. (2019a). A description of the MYNN-EDMF scheme and the coupling to other components in WRF–ARW.

Olson, J. B., Kenyon, J. S., Djalalova, I., Bianco, L., Turner, D. D., Pichugina, Y., et al. (2019b). Improving wind energy forecasting through numerical weather prediction model development. *Bulletin of the American Meteorological Society*, *100*(11), 2201–2220. https://doi.org/10.1175/bams-d-18-0040.1

Ou, T., Chen, D., Chen, X., Lin, C., Yang, K., Lai, H.-W., & Zhang, F. (2020). Simulation of summer precipitation diurnal cycles over the Tibetan Plateau at the gray-zone grid spacing for cumulus parameterization. *Climate Dynamics*, *54*(7–8), 3525–3539. https://doi.org/10.1007/s00382-020-05181-x

Prein, A. F., Langhans, W., Fosser, G., Ferrone, A., Ban, N., Goergen, K., et al. (2015). A review on regional convection-permitting climate modeling: Demonstrations, prospects, and challenges. *Reviews of Geophysics*, *53*(2), 323–361. https://doi.org/10.1002/2014rg000475

Qin, Y., & Lin, Y. (2018). Alleviated double ITCZ problem in the NCAR CESM1: A new cloud scheme and the working mechanisms. *Journal of Advances in Modeling Earth Systems*, *10*(9), 2318–2332. https://doi.org/10.1029/2018ms001343

Qin, Y., Lin, Y. L., Xu, S. M., Ma, H. Y., & Xie, S. C. (2018). A diagnostic PDF cloud scheme to improve subtropical low clouds in NCAR community atmosphere model (CAM5). *Journal of Advances in Modeling Earth Systems*, *10*(2), 320–341. https://doi.org/10.1002/2017ms001095

Qiu, J. (2008). The third pole. *Nature*, *454*(7203), 393–396. https://doi.org/10.1038/454393a

Rahimi, S. R., Wu, C., Liu, X., & Brown, H. (2019). Exploring a variable-resolution approach for simulating regional climate over the Tibetan Plateau using VR-CESM. *Journal of Geophysical Research-Atmospheres*, *124*(8), 4490–4513. https://doi.org/10.1029/2018jd028925

Ruiz-Arias, J. A., Arbizu-Barrena, C., Santos-Alamillos, F. J., Tovar-Pescador, J., & Pozo-Vázquez, D. (2016). Assessing the surface solar radiation budget in the WRF model: A spatiotemporal analysis of the bias and its causes. *Monthly Weather Review*, *144*(2), 703–711. https://doi.org/10.1175/mwr-d-15-0262.1

Ruiz-Arias, J. A., Dudhia, J., Santos-Alamillos, F. J., & Pozo-Vázquez, D. (2013). Surface clear-sky shortwave radiative closure intercomparisons in the Weather Research and Forecasting model. *Journal of Geophysical Research: Atmospheres*, *118*(17), 9901–9913. https://doi.org/10.1002/jgrd.50778

Sellers, P. J., Dickinson, R. E., Randall, D. A., Betts, A. K., Hall, F. G., Berry, J. A., et al. (1997). Modeling the exchanges of energy, water, and carbon between continents and the atmosphere. *Science*, *275*(5299), 502–509. https://doi.org/10.1126/science.275.5299.502

Shang, H., Letu, H., Nakajima, T. Y., Wang, Z., Ma, R., Wang, T., et al. (2018). Diurnal cycle and seasonal variation of cloud cover over the Tibetan Plateau as determined from Himawari-8 new-generation geostationary satellite data. *Scientific Reports*, *8*(1), 1105. https://doi.org/10.1038/s41598-018-19431-w

Shen, Y., & Xiong, A. (2016). Validation and comparison of a new gauge-based precipitation analysis over mainland China. *International Journal of Climatology*, *36*(1), 252–265. https://doi.org/10.1002/joc.4341

Sheridan, P., Smith, S., Brown, A., & Vosper, S. (2010). A simple height-based correction for temperature downscaling in complex terrain. *Meteorological Applications*, *17*(3), 329–339. https://doi.org/10.1002/met.177

Shi, G.-Y., Hayasaka, T., Ohmura, A., Chen, Z.-H., Wang, B., Zhao, J.-Q., et al. (2008). Data quality assessment and the long-term trend of ground solar radiation in China. *Journal of Applied Meteorology and Climatology*, *47*(4), 1006–1016. https://doi.org/10.1175/2007jamc1493.1

Skamarock, W. C., Klemp, J. B., Dudhia, J., Gill, D. O., Liu, Z., Berner, J., et al. (2019). A desciption of the advancd research WRF model version 4.

Sommeria, G., & Deardorff, J. W. (1977). Subgrid-scale condensation in models of nonprecipitating clouds. *Journal of the Atmospheric Sciences*, *34*(2), 344–355. https://doi.org/10.1175/1520-0469(1977)034<0344:sscimo>2.0.co;2

Su, F., Duan, X., Chen, D., Hao, Z., & Cuo, L. (2013). Evaluation of the global climate models in the CMIP5 over the Tibetan Plateau. *Journal of Climate*, *26*(10), 3187–3208. https://doi.org/10.1175/jcli-d-12-00321.1

Subin, Z. M., Riley, W. J., & Mironov, D. (2012). An improved lake model for climate simulations: Model structure, evaluation, and sensitivity analyses in CESM1. *Journal of Advances in Modeling Earth Systems*, *4*(1), M02001. https://doi.org/10.1029/2011ms000072

Sun, S., Shi, C. X., Pan, Y., Bai, L., Xu, B., Zhang, T., et al. (2020). Applicability assessment of the 1998–2018 CLDAS multi-source precipitation fusion dataset over China. *Journal of Meteorological Research*, *34*(4), 879–892. https://doi.org/10.1007/s13351-020-9101-2

Tang, W., Qin, J., Yang, K., Niu, X., Zhang, X., Yu, Y., & Zhu, X. (2013). Reconstruction of daily photosynthetically active radiation and its trends over China. *Journal of Geophysical Research-Atmospheres*, *118*(23), 13292–13302. https://doi.org/10.1002/2013jd020527

Tang, W. J., Yang, K., Qin, J., Cheng, C. C. K., & He, J. (2011). Solar radiation trend across China in recent decades: A revisit with quality-controlled data. *Atmospheric Chemistry and Physics*, *11*(1), 393–406. https://doi.org/10.5194/acp-11-393-2011

Thompson, G., Field, P. R., Rasmussen, R. M., & Hall, W. D. (2008). Explicit forecasts of winter precipitation using an improved bulk microphysics scheme. Part II: Implementation of a New Snow Parameterization. *Monthly Weather Review*, *136*(12), 5095–5115. https://doi.org/10.1175/2008mwr2387.1

Thompson, G., Tewari, M., Ikeda, K., Tessendorf, S., Weeks, C., Otkin, J., & Kong, F. (2016). Explicitly-coupled cloud physics and radiation parameterizations and subsequent evaluation in WRF high-resolution convective forecasts. *Atmospheric Research*, *168*, 92–104. https://doi.org/10.1016/j.atmosres.2015.09.005

Tompkins, A. M. (2005). *The parametrization of cloud cover (technical memorandum)*. European Center for Medium-Range Weather Forecasts.

Wang, L., Yao, T., Chai, C., Cuo, L., Su, F., Zhang, F., et al. (2021). TP-River: Monitoring and quantifying total river runoff from the Third Pole. *Bulletin of the American Meteorological Society*, *102*(5), 1–45. https://doi.org/10.1175/bams-d-20-0207.1

Wang, X., Pang, G., & Yang, M. (2018). Precipitation over the Tibetan Plateau during recent decades: A review based on observations and simulations. *International Journal of Climatology*, *38*(3), 1116–1131. https://doi.org/10.1002/joc.5246

Wang, X., Tolksdorf, V., Otto, M., & Scherer, D. (2021). WRF-based dynamical downscaling of ERA5 reanalysis data for High Mountain Asia: Towards a new version of the High Asia Refined analysis. *International Journal of Climatology*, *41*(1), 743–762. https://doi.org/10.1002/joc.6686

Wang, Y., Yang, K., Zhou, X., Chen, D., Lu, H., Ouyang, L., et al. (2020a). Synergy of orographic drag parameterization and high resolution greatly reduces biases of WRF-simulated precipitation in central Himalaya. *Climate Dynamics*, *54*(3–4), 1729–1740. https://doi.org/10.1007/s00382-019-05080-w

Wang, Y., Zeng, X., Xu, X., Welty, J., Lenschow, D. H., Zhou, M., & Zhao, Y. (2020b). Why are there more summer afternoon low clouds over the Tibetan Plateau compared to eastern China? *Geophysical Research Letters*, *47*(23), e2020GL089665. https://doi.org/10.1029/2020gl089665

Wu, G., Ma, T., Liu, Y., & Jiang, Z. (2020). PV-Q perspective of cyclogenesis and vertical velocity development downstream of the Tibetan Plateau. *Journal of Geophysical Research-Atmospheres*, *125*(16), e2019JD030912. https://doi.org/10.1029/2019jd030912

Wu, P., Christidis, N., & Stott, P. (2013). Anthropogenic impact on Earth's hydrological cycle. *Nature Climate Change*, *3*(9), 807–810. https://doi.org/10.1038/nclimate1932

Xu, K. M., & Randall, D. A. (1996). A semiempirical cloudiness parameterization for use in climate models. *Journal of the Atmospheric Sciences*, *53*(21), 3084–3102. https://doi.org/10.1175/1520-0469(1996)053<3084:ascpfu>2.0.co;2

Xu, X., Lu, C., Liu, Y., Gao, W., Wang, Y., Cheng, Y., et al. (2020). Effects of cloud liquid-phase microphysical processes in mixed-phase cumuli over the Tibetan Plateau. *Journal of Geophysical Research-Atmospheres*, *125*(19), e2020JD033371. https://doi.org/10.1029/2020jd033371

Xu, X., Lu, C., Shi, X., & Gao, S. (2008). World water tower: An atmospheric perspective. *Geophysical Research Letters*, *35*(20), L20815. https://doi.org/10.1029/2008gl035867

Xu, X., Ma, Y., Sun, C., & Wei, F. (2019). Effect of energy and water circulation over Tibetan Plateau. *Bulletin of the Chinese Academy of Sciences*, *34*(11), 1293–1305.

Xu, X., Zhou, M., Chen, J., Bian, L., Zhang, G., Liu, H., et al. (2002). A comprehensive physical pattern of land-air dynamic and thermal structure on the Qinghai-Xizang Plateau. *Science in China - Series D: Earth Sciences*, *45*(7), 577–594. https://doi.org/10.1360/02yd9060

Yang, K., Tang, Q., & Lu, H. (2022). Precipitation recycling ratio and water vapor sources on the Tibetan Plateau. *Science China Earth Sciences*, *65*(3), 584–588. https://doi.org/10.1007/s11430-021-9871-5

Yang, K., & Wang, C. H. (2019). Water storage effect of soil freeze-thaw process and its impacts on soil hydro-thermal regime variations. *Agricultural and Forest Meteorology*, *265*, 280–294. https://doi.org/10.1016/j.agrformet.2018.11.011

Yang, K., Wang, C. H., & Li, S. Y. (2018). Improved simulation of frozen-thawing process in land surface model (CLM4.5). *Journal of Geophysical Research: Atmospheres*, *123*(23), 13238–13258. https://doi.org/10.1029/2017jd028260

Yang, K., Wu, H., Qin, J., Lin, C. G., Tang, W. J., & Chen, Y. Y. (2014). Recent climate changes over the Tibetan Plateau and their impacts on energy and water cycle: A review. *Global and Planetary Change*, *112*, 79–91. https://doi.org/10.1016/j.gloplacha.2013.12.001

Yao, T., Xue, Y., Chen, D., Chen, F., Thompson, L., Cui, P., et al. (2019). Recent third pole's rapid warming accompanies cryospheric melt and water cycle intensification and interactions between monsoon and environment: Multidisciplinary approach with observations, modeling, and analysis. *Bulletin of the American Meteorological Society*, *100*(3), 423–444. https://doi.org/10.1175/bams-d-17-0057.1

Ye, D. Z. (1981). Some characteristics of the summer circulation over the Qinghai-Xizang (Tibet) plateau and its neighborhood. *Bulletin of the American Meteorological Society*, *62*(1), 14–19. https://doi.org/10.1175/1520-0477(1981)062<0014:scotsc>2.0.co;2

Yun, Y., Liu, C., Luo, Y., Liang, X., Huang, L., Chen, F., & Rasmmusen, R. (2020). Convection-permitting regional climate simulation of warm-season precipitation over eastern China. *Climate Dynamics*, *54*(3), 1469–1489. https://doi.org/10.1007/s00382-019-05070-y

Zhang, G. Q., Luo, W., Chen, W. F., & Zheng, G. X. (2019). A robust but variable lake expansion on the Tibetan Plateau. *Science Bulletin*, *64*(18), 1306–1309. https://doi.org/10.1016/j.scib.2019.07.018

Zhao, D., Dong, W., Lin, Y., Hu, Y., & Cao, D. (2022). Diurnal variation of precipitation over the high mountain Asia: Spatial distribution and its seasonality. *Journal of Hydrometeorology*, *23*(12), 1945–1959. https://doi.org/10.1175/jhm-d-21-0243.1

Zhao, D., Lin, Y., Li, Y., & Gao, X. (2021). An extreme heat event induced by Typhoon Lekima (2019) and its contributing factors. *Journal of Geophysical Research: Atmospheres*, *126*(11), e2021JD034760. https://doi.org/10.1029/2021jd034760

Zhao, F., Xiong, A., Zhang, X., Deng, L., Wang, Y., Ma, Q., et al. (2017). Technical characteristics of the architecture design of China integrated meteorological information sharing system. *Journal of Applied Meteorolgical Science*, *28*(6), 750–758.

Zhao, P., Zhou, X. J., Chen, J. M., Liu, G., & Nan, S. L. (2019). Global climate effects of summer Tibetan Plateau. *Science Bulletin*, *64*(1), 1–3. https://doi.org/10.1016/j.scib.2018.11.019

Zhao, Y., Zhou, T., Li, P., Furtado, K., & Zou, L. (2021). Added value of a convection permitting model in simulating atmospheric water cycle over the Asian water tower. *Journal of Geophysical Research: Atmospheres*, *126*(13), e2021JD034788. https://doi.org/10.1029/2021jd034788

Zhou, X., Yang, K., Beljaars, A., Li, H., Lin, C., Huang, B., & Wang, Y. (2019). Dynamical impact of parameterized turbulent orographic form drag on the simulation of winter precipitation over the western Tibetan Plateau. *Climate Dynamics*, *53*(1–2), 707–720. https://doi.org/10.1007/s00382-019-04628-0

Zhou, X., Yang, K., Ouyang, L., Wang, Y., Jiang, Y., Li, X., et al. (2021). Added value of kilometer-scale modeling over the third pole region: A CORDEX-CPTP pilot study. *Climate Dynamics*, *57*(7–8), 1673–1687. https://doi.org/10.1007/s00382-021-05653-8

Zhou, X., Yang, K., & Wang, Y. (2018). Implementation of a turbulent orographic form drag scheme in WRF and its application to the Tibetan Plateau. *Climate Dynamics*, *50*(7–8), 2443–2455. https://doi.org/10.1007/s00382-017-3677-y

Zhu, Y.-Y., & Yang, S. (2020). Evaluation of CMIP6 for historical temperature and precipitation over the Tibetan Plateau and its comparison with CMIP5. *Advances in Climate Change Research*, *11*(3), 239–251. https://doi.org/10.1016/j.accre.2020.08.001